Correction published 22 November 2003

Simulation of hydrologic changes associated with global warming

Richard T. Wetherald

Geophysical Fluid Dynamics Laboratory/NOAA, Princeton, New Jersey, USA

Syukuro Manabe[1]

Frontier Research System for Global Change, Kanagawa, Japan

[1] Using the results obtained from a coupled ocean-atmosphere-land model with medium computational resolution, we investigated how the hydrology of the continents changes in response to the combined increases of greenhouse gases and sulfate aerosols in the atmosphere, which are determined based upon the IS92a scenario. In order to extract the forced response from natural, internal variability, the difference between the mean of an eight-member ensemble of numerical experiments and a control experiment are used for the present analysis. The global mean surface air temperature of the coupled model increases by about 2.3°C above the preindustrial level by the middle of the 21st century. Accompanying the warming, the global mean rates of both precipitation and evaporation increase by 5.2%, yielding the average increase in the rate of runoff by approximately 7.3%. The increase in the rate of runoff simulated by the model is particularly large in high northern latitudes, where the runoff from some rivers such as the Mackenzie and Ob′ may increase by as much as 20%. Runoff from many European rivers increases by more than 20%. Runoff also increases substantially in some tropical rivers such as the Amazon and Ganges. However, the percentage changes in simulated runoff from many other tropical rivers and middle latitude rivers are smaller with both positive and negative signs. In middle and high latitudes in the Northern Hemisphere, soil moisture tends to decrease in summer, whereas it increases in winter. However, in many semi-arid regions in subtropical and middle latitudes, soil moisture is reduced during most of a year. These semi-arid regions include the southwestern part of North America, the northeastern part of China in the Northern Hemisphere, and the region in the vicinity of the Kalahari Desert and southern part of Australia in the Southern Hemisphere. Since a semi-arid region usually surrounds a desert, the reduction of soil moisture in such a region often results in the expansion of the desert. Soil moisture is also reduced during the dry season in many semi-arid regions. For example, it is reduced in the savannahs of Africa and South America during winter and early spring in the Southern Hemisphere. In the Northern Hemisphere, it is reduced at the Mediterranean coast of Europe in summer. *INDEX TERMS:* 1860 Hydrology: Runoff and streamflow; 1866 Hydrology: Soil moisture; 3309 Meteorology and Atmospheric Dynamics: Climatology (1620); 3322 Meteorology and Atmospheric Dynamics: Land/atmosphere interactions; 3354 Meteorology and Atmospheric Dynamics: Precipitation (1854); *KEYWORDS:* global warming, coupled ocean-atmosphere models, climate models, soil moisture changes, runoff changes, drought

1. Introduction

[2] In the preceding study, *Wetherald and Manabe* [1999] investigated the change in land surface hydrology of a coupled atmosphere-ocean-land model, which occurs in response to the combined changes of greenhouse gases and sulfate aerosols [*Haywood et al.*, 1997]. However, because of the coarse computational resolution of the coupled model used, the geographical distribution of precipitation simulated by the model was not realistic enough to reliably evaluate in detail the changes in the hydrology of the continents, which accompany global warming.

[3] During the last several years, the staff members of Geophysical Fluid Dynamics Laboratory (GFDL) of NOAA [e.g., *Knutson et al.*, 1999] repeated the numerical experiment conducted by *Haywood et al.* [1997], using a version of the coupled model, which has approximately twice as high a resolution as the original version. Fortunately, this

---

[1]Now at Program in Atmospheric and Oceanic Sciences, Princeton University, Princeton, New Jersey, USA.

medium resolution version of the coupled model reproduces the observed, broad-scale distribution of precipitation substantially better than the low-resolution version of the coupled model used in our previous study. This is one of the important reasons why we repeated our previous study.

[4] Another important factor, which motivates the present study, is the very large unforced, natural variability of the continental hydrology simulated by the model. To distinguish radiatively forced change from the unforced change of a hydrologic variable, we use the results from the ensemble of the eight global warming experiments conducted recently by the staff members of GFDL. In this respect, the present study differs from our previous study, which was based upon the result from a single global warming experiment. Averaging the results from the ensemble of the eight global warming experiments, we reduced the influence of unforced, natural variability, thereby extracting the radiatively forced hydrologic changes.

[5] In the previous studies, the main emphasis has been placed upon the midcontinental change of soil moisture during summer and winter. To study the reduction in soil moisture in the semi-arid regions of the world, which occurs during much of a year, we examine here the changes of soil moisture over an entire annual cycle.

2. Coupled Atmosphere-Ocean-Land Model
2.1. Brief Description of the Model

[6] *Manabe et al.* [1991] described the basic structure of the model used here. It consists of general circulation models (GCM) of the atmosphere and oceans, and a simple model of the surface layer of the continents. It is a global model with realistic geography limited by its computational resolution. The vertical transfer of sensible and latent heat through moist convection is represented by a simple scheme called "moist convective adjustment" [*Manabe et al.*, 1965]. The model insolation has seasonal variation. However, diurnal variation of insolation is not included for simplicity and computational economy. The model predicts cloud cover, which depends only on relative humidity. A so-called "bucket model" [*Manabe*, 1969] is used to compute the budget of water in soil. To facilitate the interpretation of the results obtained, the bucket model was constructed as simple as possible. For example, it is assumed that the field capacity of soil is 15 cm everywhere and the minimum value of soil moisture at the wilting point is zero. In addition, it is assumed that the rate of evaporation (E) increases with increasing soil moisture (W), and attains the rate of potential evaporation (E_P) when soil moisture reaches 75% (or higher) of saturation (W_{FC}). Following *Milly* [1992], the potential evaporation rate (E_P) is defined in a manner, which is different from the original bucket model. It is given by

$$E_P = \rho \cdot L \cdot C_D \cdot | V_a | \cdot [r_s(T_W) - r_a] \qquad (1)$$

where ρ, C_D, $|V_a|$, and r_a are density of air, drag coefficient, wind velocity, and mixing ratio of water vapor, respectively, at the lowest finite difference level of the model atmosphere located at an altitude of $\sim$25 m. L is the latent heat of condensation. The $r_s(T_W)$ is the mixing ratio of water vapor in saturated air, which has temperature T_W of the hypothetically wet surface.

[7] For the sake of simplicity, it is assumed that water runs off only when the field capacity of soil is exceeded. With regard to river discharge, the total runoff at the mouth of each river is computed by summing the runoff from all grid boxes in the drainage basin of the river. K. A. Dunne of GFDL (personal communication) determined the geographical extent of a basin using the Time Atlas of the World (1988). (See Figure 8 in section 3 for the map of drainage basins she constructed.)

[8] The oceanic GCM [*Bryan and Lewis*, 1979] uses a finite-difference technique and has a regular grid system. This oceanic component of the coupled model interacts with the atmospheric counterpart once each day through the exchange of heat, water, and momentum. A simple sea ice model is also incorporated into the oceanic GCM. Based upon the requirement of thermodynamic heat balance, the sea ice model predicts the thickness of sea ice, which moves with surface ocean currents so long as its thickness is less than 4 m. For the description of the coupled ocean-atmosphere-land model, which is hereinafter called "coupled model" for simplicity, see *Manabe et al.* [1991].

[9] Recently, *Delworth et al.* [2002] documented the current version of the coupled model used here, which has approximately twice as high a horizontal resolution as the original version described by *Manabe et al.* [1991]. In this new version, the global distributions of predicted variables in the atmospheric component of the model are represented by spherical harmonics of 30 associated Legendre functions for each of 30 Fourier components and by grid point values [*Gorden and Stern*, 1982]. It has 14 vertical finite-difference levels. The oceanic component of the model has 18 vertical finite difference levels and a regular horizontal grid system with approximately ($2°$ latitude) and ($1.8°$ longitude) intervals. Most of the coefficients of viscosity and diffusion due to subgrid-scale eddies are substantially smaller than those used in the low-resolution model constructed earlier.

[10] In conducting the control and climate change experiments, which are described in the following subsections, *Delworth et al.* [2002] employ two versions of their coupled model, which differs in the specification of sub-grid scale mixing of heat and salt. With the exception of the northern North Atlantic Ocean, the global distribution of sea surface temperature obtained from the control integration is almost identical between the two versions of the model. To increase the number of the global warming experiments available for our analysis, we decided to analyze the ensemble of eight climate change experiments (i.e., three from the first version and five from the second version of the model) as if they were obtained from an identical model. To inspect the distributions of sea surface temperature obtained from the two versions of the coupled model, see *Delworth et al.* [2002].

2.2. Control Experiment

[11] The initial condition for the time integration of the coupled model was obtained from the separate time integrations of the atmospheric and oceanic components of the coupled model. For the integration of the atmospheric component, the observed distribution of sea surface temperature is used as a lower boundary condition. For the oceanic integration, the observed distributions of sea surface temperature and sea surface salinity, and the computed

distribution of surface wind stress, which is obtained from the atmospheric component of the model, are used as upper boundary conditions. Both integrations are performed long enough for the model to approach very closely to the states of equilibrium. Combining the quasi-equilibrium states of the atmospheric and oceanic components thus obtained, we constructed the initial condition for the time integration of the coupled model.

[12] When the time integration of a coupled model starts from the initial conditions thus obtained, the model climate usually drifts toward its own equilibrium state. Such a drift makes the distributions of sea ice, surface temperature, and surface salinity less realistic, distorting the sensitivity of a model climate. To reduce the drift, the fluxes of heat and water at the ocean-atmosphere interface are adjusted by given amounts, which varies geographically and seasonally, before they are imposed upon the oceanic surface (see *Manabe et al.* [1991] for details). These adjustments, however, do not change from one year to the next, and are independent of the anomalies of sea surface temperature and salinity, which develop during a time integration of the coupled model. Thus they neither systematically damp nor amplify the surface anomalies. Obviously, the adjustment does not eliminate the shortcomings of the model dynamics or thermodynamics [*Marotzke and Stone*, 1995]. However, they help to prevent very harmful drift of the model from a realistic initial condition.

[13] There is no doubt that it is highly desirable to develop a coupled model that maintains a realistic control climate without employing the technique of the flux adjustment as proposed, for example, by *Gregory and Mitchell* [1997]. However, the simulated thickness of sea ice in their model appears to be too thin over the Arctic Ocean [*Vinnikov et al.*, 1999], reducing the albedo feedback effect in their global warming experiment. Until a perfectly realistic model becomes available, the technique of flux adjustment is a useful alternative.

[14] Using the initial condition, which is constructed as described above, the control integration of the coupled model is performed over a period of approximately 1000 years. Eliminating the initial 100-year period when the model has a small but systematic trend, we analyzed the results from the last 900 years of the integration. Owing to the flux adjustment, the horizontal distributions of the temperature and salinity at oceanic surface remain realistic throughout the course of the control integration.

2.3. Simulated Land Surface Hydrology

[15] In order to evaluate the skill of the model in simulating the hydrologic cycle, this subsection illustrates the geographical distributions of selected hydrologic variables obtained from the control integration. In Figure 1, the distribution of annual mean rate of simulated precipitation is compared with that of the observed precipitation. This comparison reveals that the model tends to underestimate tropical rainfall in the Indian and Atlantic Oceans and eastern part of Pacific Ocean. Nevertheless, the model simulates approximately the broad-scale features of precipitation over the world.

[16] The geographical distribution of simulated annual mean precipitation shown in Figure 1 is more realistic than what was obtained from the low-resolution version of the model used in the earlier study by *Wetherald and Manabe* [1999]. In general, the low-resolution version of the coupled model tends to overestimates precipitation over the continents in middle latitudes. In low latitudes, it tends to underestimate tropical precipitation and to overestimate the meager precipitation in the subtropics (see, for example, Figures 2 and 3 of *Manabe et al.* [1992]).

[17] The simulated distribution of precipitation, in turn, affects that of soil moisture. Figure 2 illustrates the simulated distribution of annual mean soil moisture obtained in the present study. It shows that the regions of very low soil moisture in the model simulation correspond reasonably well with the major arid regions of the world: the Gobi and Thar Deserts of Eurasia, the Mojave Desert of North America, the Patagonian Desert of South America, and the Sahara and Kalahari Deserts of Africa. The regions of relatively low soil moisture simulated by the model also correspond approximately to many semi-arid regions of the world such as the western plains of North America, the northeastern region of China, the Mediterranean coast of Europe, and the grasslands of Africa, South America, and Australia.

2.4. Climate Change Experiments

[18] The climate change experiments used in this study comprises an eight-member ensemble of numerical experiments of the coupled model, which are radiatively forced by increasing equivalent greenhouse gases and sulfate aerosols over the period 1865 to 2090. Each member of the ensemble began from a different initial condition, which was taken from the control run conditions at least 40 years apart. The radiative forcing of the coupled model is identical to what was used by *Haywood et al.* [1997]. It was determined using the estimates of past, present and future equivalent carbon dioxide concentration and sulfate loading, and is similar to the IS92a scenario of *Intergovernmental Panel on Climate Change* (*IPCC*) [1992]. For the 21st century, it belongs to the lower half of the range of the more recent SRES scenarios compiled recently by the *IPCC* [2000].

[19] The simulated increase of annual mean, global mean surface air temperature obtained from the climate change experiments is approximately 2.3°C by the middle of the next century. The magnitude of the increase is slightly smaller than what *Haywood et al.* [1997] obtained using a version of the coupled model, which has approximately twice as low a resolution as the version used in the present study. With the exception of the Arctic Ocean, where the increase of surface air temperature is two to three times as large as its global average due to the albedo feedback effect of sea ice, the increase is relatively large over continents as compared with the ocean (Figure 3). In sharp contrast to Arctic Ocean, the warming is small in the Circumpolar Ocean of the Southern Hemisphere. In general, the geographical distribution of surface temperature change described above is qualitatively similar to what *Manabe et al.* [1991] obtained and discussed in detail.

[20] The time series of global mean surface air temperature and global mean rates of precipitation, which are obtained from the ensemble of the eight climate change experiments, are illustrated in Figure 4. This figure shows that not only global mean surface air temperature but also global mean rate of precipitation increases systematically. Superposed upon the systematic increase by the end of the
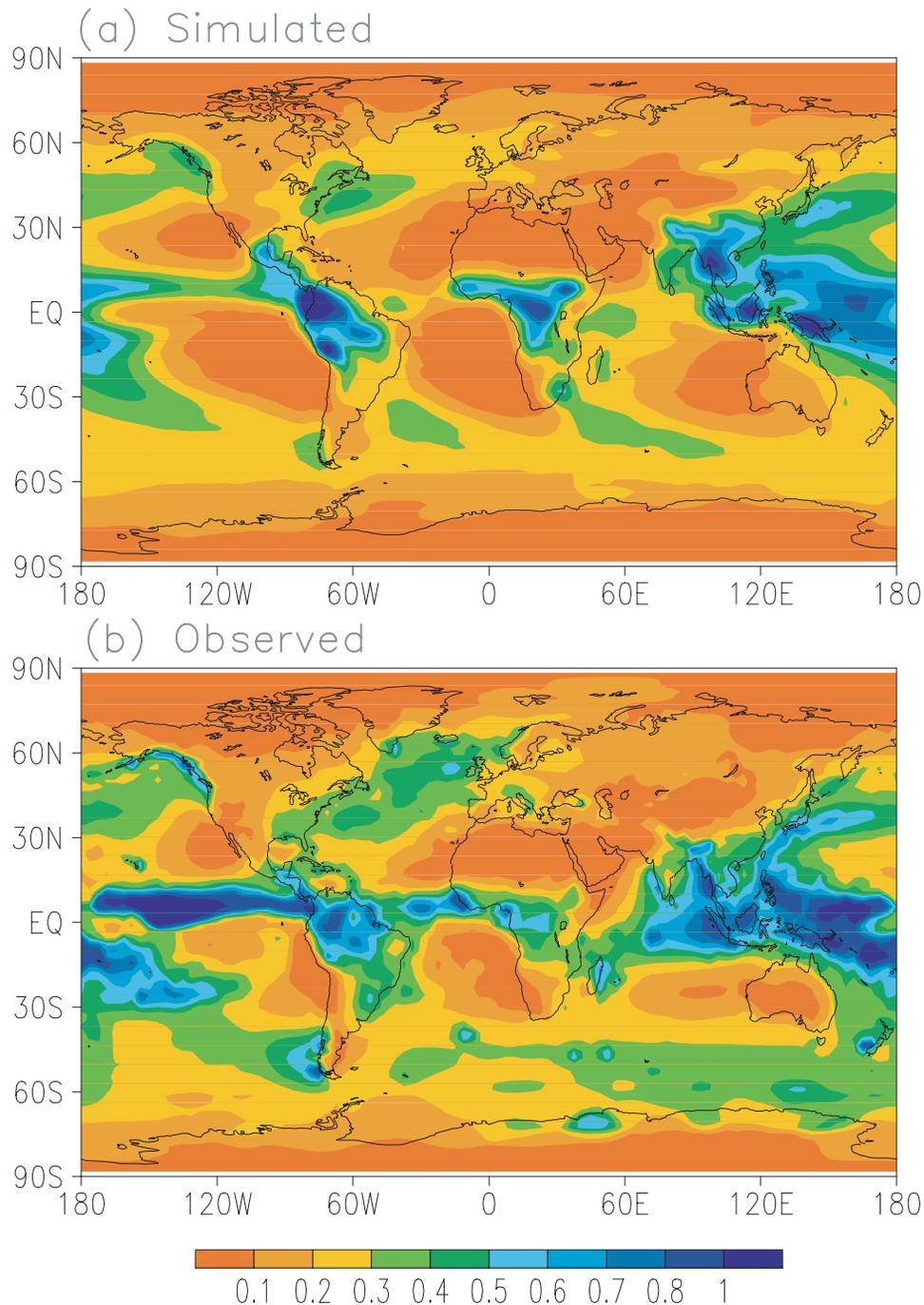
Figure 1. Geographical distribution of annual mean rate of precipitation (cm/day). (a) Control experiment. (b) Observed [*Legates and Willmott*, 1990].

21st century (signal), there is a large natural variability (noise) for both of these variables. The signal to noise ratio, however, is much smaller for the global mean rate of precipitation than for global mean surface air temperature. Nevertheless, the total increases of global mean precipitation rate by the end of the 21st century (signal) are larger than the standard deviation of its natural variability (noise). A similar statement does not apply to local precipitation. Though it is not shown here, unforced, natural variability (noise) is usually comparable to or larger than the radiatively forced, systematic change of local precipitation, which occurs by the end of the 21st century (signal).

[21] The large natural variability in local precipitation, in turn, induces a large variability in local soil moisture, which is comparable to or larger than its systematic change (see, for example, Figure 13, which illustrates the time series of annual mean soil moisture averaged over a large area in the southwestern part of the North American Continent). To extract the signal of the radiatively forced changes, we averaged the results from the eight- member ensemble of the climate change experiments. The result from each member of the ensemble is obtained by averaging the time series of a hydrologic variable over the 30-year period between the years 2035 and 2065. Thus a
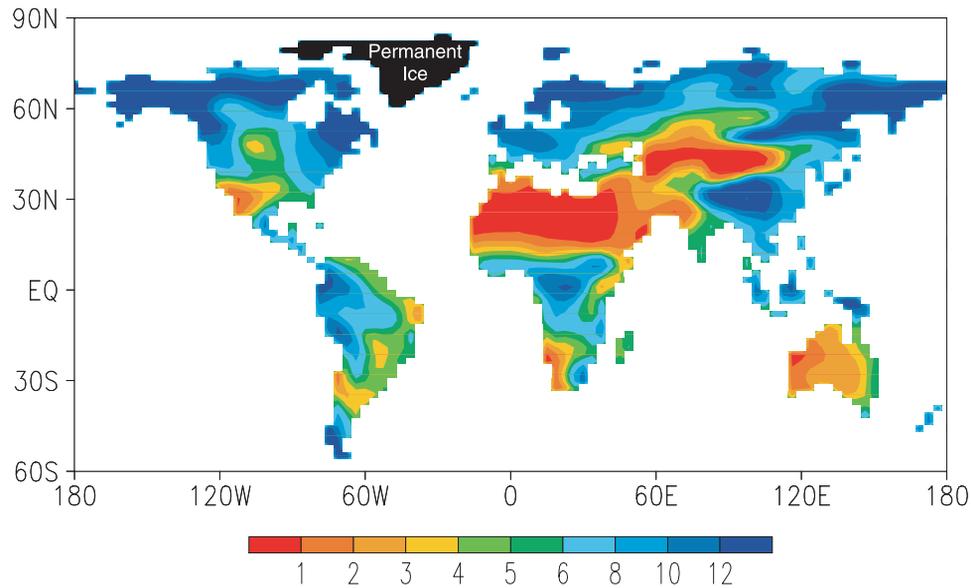
Figure 2. Geographical distribution of annual mean soil moisture (cm) obtained from the control experiment.

variable obtained from the climate change experiments represents an average taken over an equivalent period of 240 years. The forced changes, which are expected from the preindustrial to the middle of 21st century, are then obtained by subtracting the 900-year mean values of the control experiment from the 240-year (240 = 8 × 30) mean values of the eight-member ensemble of the climate change experiments. We expect that the averaging facilitates the extraction of the radiatively forced change, reducing the contribution from the unforced natural variability.

[22] The simulated changes of various variables from the preindustrial to the middle of the 21st centuries are the

subject of extensive discussion in this study. Unless specified otherwise, they are computed as described in the preceding paragraph, using the outputs from the control and the eight-member ensemble of the climate change experiments.

3.   Change in River Runoff

[23] Figure 4 shows that the systematic change of the global mean rate of precipitation resembles that of global mean surface temperature. As global mean surface temperature increases, the saturation vapor pressure at oceanic and continental surface increases, thereby enhancing both evap-
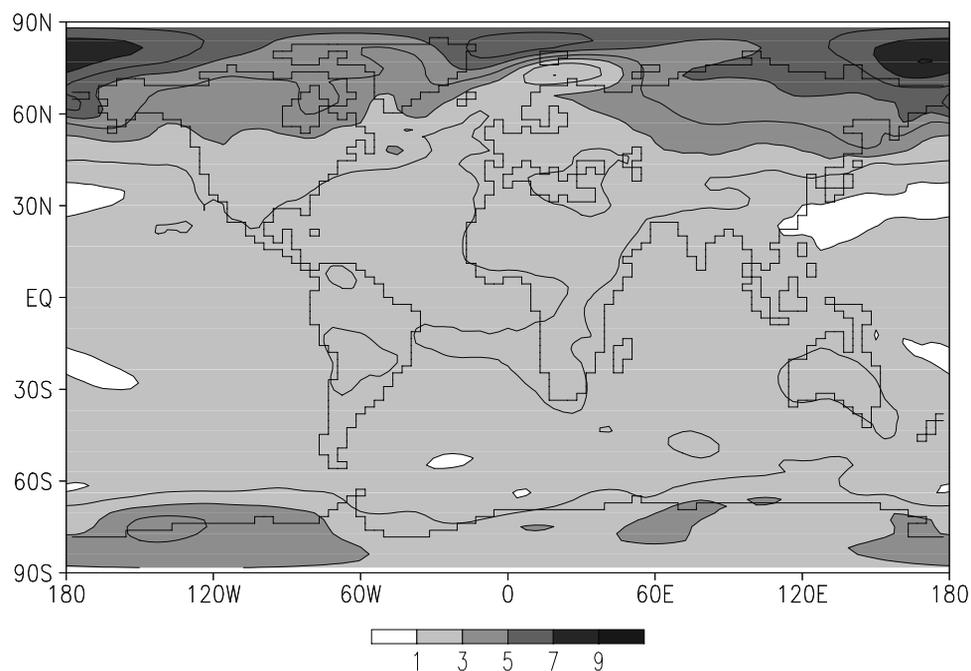
Figure 3. Geographical distribution of the simulated change in annual mean surface air temperature (°C) from the preindustrial to the middle of the 21st century.
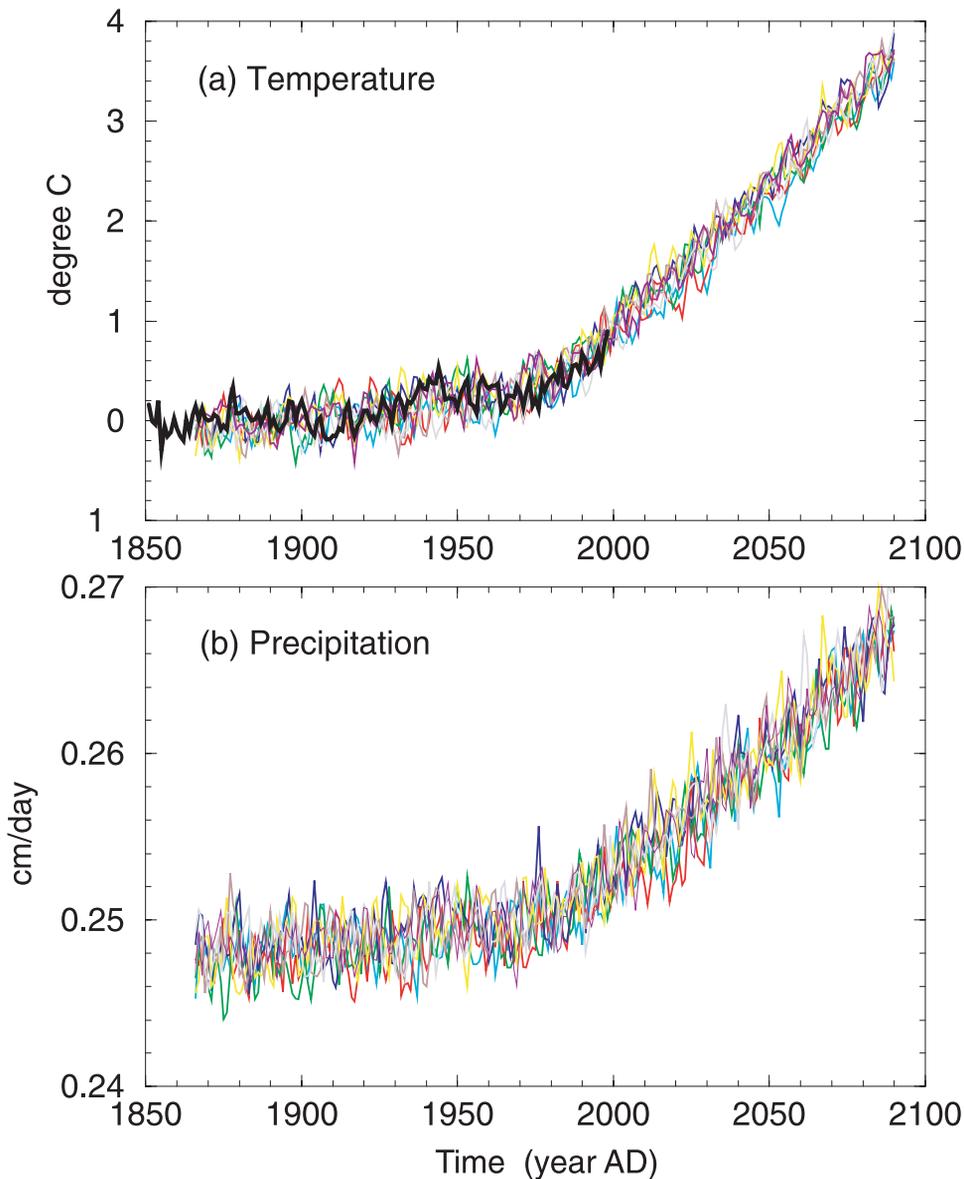
Figure 4. Time series of (a) globally averaged, annual mean surface air temperature anomaly (°C), and (b) globally averaged, annual mean rate of precipitation (cm/day), which are obtained from an ensemble of the eight climate change experiments. The thick black line in Figure 4a indicates a time series of observed annual mean, global mean surface air temperature, which was constructed and updated by *Jones and Wigley* [1991].

oration and precipitation. By the year 2050, global mean rates of annual precipitation and evaporation increase by an identical 5.2% (Table 1). Because the spatial and temporal variability of precipitation is much larger than that of evaporation, a given percentage increase in precipitation often results in larger increase in river runoff. The percentage increase in the annual mean rate of runoff averaged over all continents turns out to be 7.3% as indicated in Table 1.

[24] The geographical distribution of the change in runoff, which occurs by the middle of the 21st century, is shown in Figure 5a. In general, the increase in the rate of runoff is relatively large in high-latitude regions of both the Eurasian and North American continents, particularly in western Europe and the northwest coast of North America.

It also increases markedly over certain regions of tropical continents, where runoff is large.

[25] The statistical significance of the runoff change shown in Figure 5a is evaluated using a two-tailed "student-t" test and is illustrated in Figure 5b. The computational procedure used here is identical to that described by *Panofsky and Brier* [1968]. The analysis is conducted over the eight 30-year segments (between 2035 and 2065) from the eight global change experiments and thirty 30-year segments from the 900-year control integration. The data of these segments yield 36 (= 30 + 8 − 2) degrees of freedom for the analysis. Statistical significance is evaluated at three confidence levels i.e., 95%, 99%, and 99.9%, and is illustrated in Figure 5b. This figure shows that the increase in runoff is statistically significant at the 99% or higher level

Table 1. Global Mean Rates of Simulated Annual Precipitation, Annual Evaporation, and Annual Runoff[a]

	Control	2035–2065	Change (%)
Global mean precipitation	90.2 cm/yr	95.0 cm/yr	4.8 cm/yr (5.2)
Global mean evaporation	90.2 cm/yr	95.0 cm/yr	4.8 cm/yr (5.2)
Mean continental runoff	39.8 cm/yr	42.7 cm/yr	2.9 cm/yr (7.3)

[a] Precipitation and evaporation averaged over the entire globe, and runoff averaged over all continents, are listed for the control experiment and the middle of the 21st century for the climate change experiments. In addition, the change and percentage change from the preindustrial to the middle of the 21st century are listed.

over a major fraction of continental regions in high latitudes and over certain tropical river basins in low latitudes.

[26] In order to comprehend the latitudinal dependence of runoff, it is desirable to examine the latitudinal profiles of precipitation and evaporation, which are obtained from the control and global warming experiments. These profiles are shown in Figure 6. This figure indicates that the rate of evaporation is small in high latitudes, because solar energy available for evaporation is small. Since extra-tropical cyclones in the atmosphere transport water vapor from subtropical to higher latitudes, precipitation exceeds evaporation substantially in middle and high latitudes (compare

Figures 6a and 6b), yielding relatively large runoff over the continents (Figure 5a). On the other hand, the meridionally overturning, Hadley Circulation brings a large amount of water vapor from the subtropics to the tropical rain belt, where heavy precipitation often exceeds evaporation, yielding a large amount of runoff in certain regions of tropics (Figure 5a).

[27] As the temperature increases in the troposphere accompanying global warming, the saturation vapor pressure, i.e., the moisture-holding capacity of air also increases, resulting in an increase of the absolute humidity of air. Thus the net export of water vapor from the subtropics increases, contributing to the increase in runoff in both high latitudes and certain regions of tropics (e.g., the Amazon River basin in Brazil and Ganges River basin in southern Asia).

[28] In their analysis of a simulated tropical circulation, *Knutson and Manabe* [1995] found that the intensity of the Hadley Circulation hardly changes, accompanying global warming. It is therefore likely that the increase in tropical precipitation is attributable mainly to the increase in moisture content of air rather than the intensification of the Hadley Circulation.

[29] Figures 6a and 7a indicate that, accompanying global warming, evaporation increases much more in low than in high latitudes. In low latitudes, where surface temperature
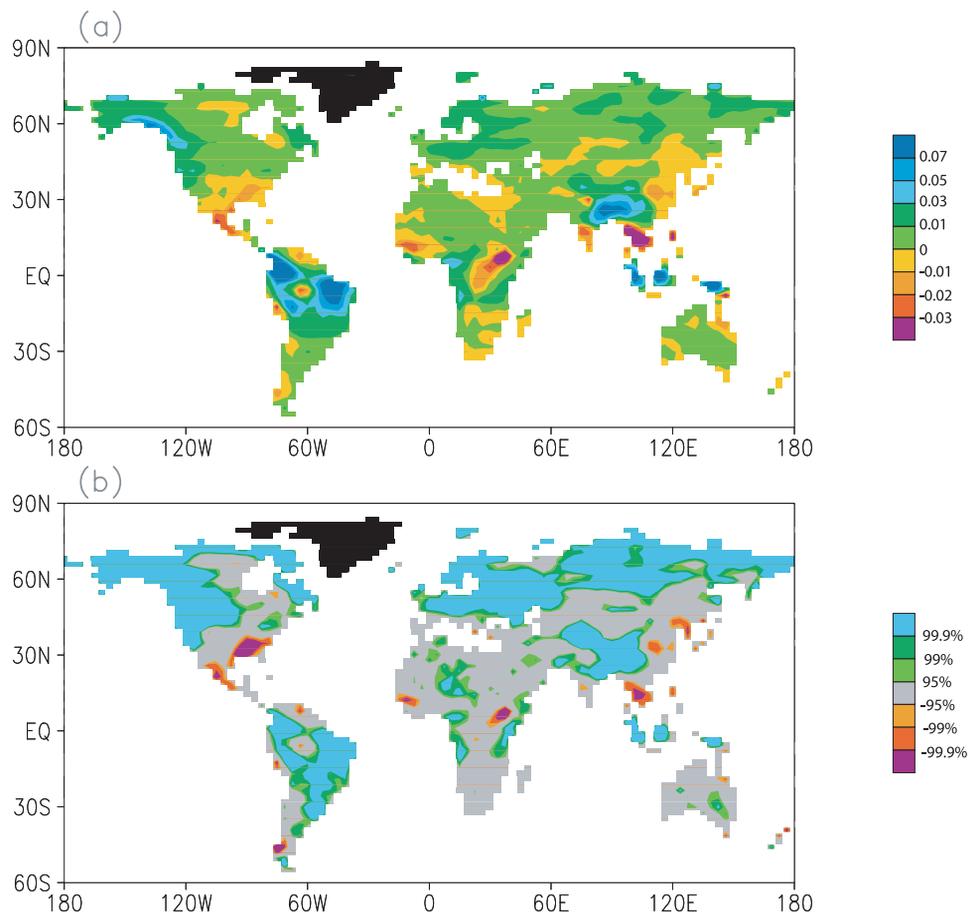
Figure 5. (a) Geographical distribution of the simulated change in the annual mean rate of runoff (cm/day) from the preindustrial to the middle of the 21st century. (b) Geographical distribution of the statistical significance of the change in annual mean rate of runoff. It is color-coded at 95%, 99%, 99.9% confidence levels.
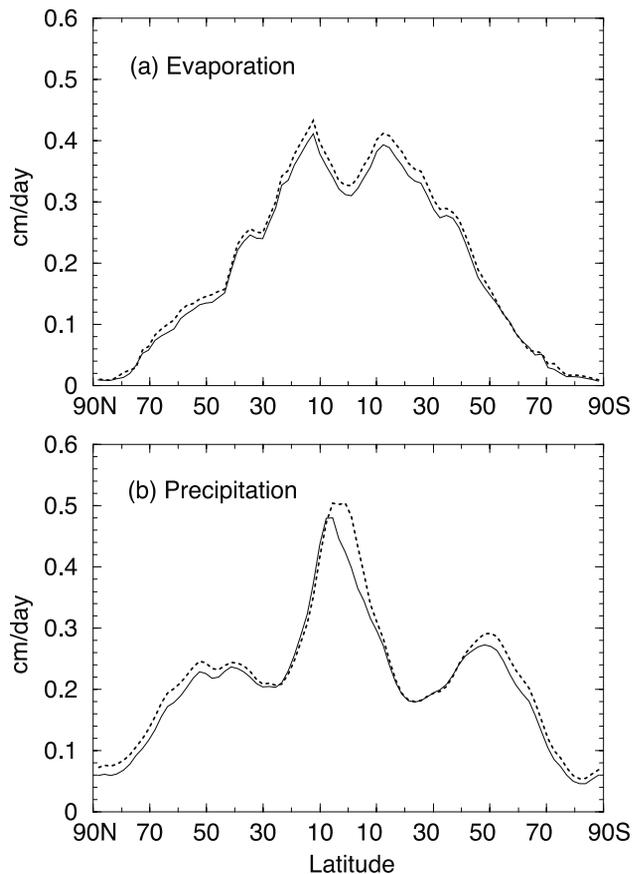
Figure 6. The latitudinal profiles of annual mean, zonal mean rates (cm/day) of (a) evaporation and (b) precipitation. Solid and dotted lines indicate the profiles obtained, averaging over the last 900-year period of the control and the 2035–2065 periods of the eight climate change experiments, respectively.

and associated saturation vapor pressure are relatively high, evaporation increases sharply with increasing surface temperature. Thus the heating due to the increase in downward flux of infrared radiation, which results from the increase of greenhouse gases in the atmosphere, contributes mostly to the increase of latent heat of evaporation rather than that of sensible heat flux. On the other hand, in high latitudes, where surface temperature and its saturation vapor pressure is low, evaporation hardly increases with increasing surface temperature. Thus the heating due to the increase in the downward flux of infrared radiation contributes mostly to the increase in sensible heat flux rather than latent heat of evaporation. Therefore evaporation hardly increases in high latitudes accompanying global warming. On the other hand, precipitation increases substantially in both low and high latitudes as discussed in the preceding paragraph. This is why the rate of runoff increases substantially in high latitudes and in certain tropical river basins (Figure 5a).

[30] The latitudinal profiles of the differences in the rates of precipitation and evaporation between the global warming and control experiments are shown in Figure 7 with a magnified scale. In this figure, the differences are zonally averaged not only over an entire latitude circle but also over all continents, and are shown in Figures 7a and 7b, respec-

tively. It clearly indicates that the latitudinal profiles of the differences in evaporation and precipitation over continents are qualitatively similar to the profiles zonally averaged over an entire latitude circle, which are discussed in the proceeding paragraph.

[31] Accompanying global warming, the rate of runoff hardly increases (or even decreases slightly) in certain areas of middle and low latitudes such as the region surrounding the Mediterranean Sea, southwestern part of North America, eastern part of China, and Indochina. In these regions, soil moisture is reduced during much of a year as discussed in the following sections.

[32] For both the control and the climate change experiments, Table 2 tabulates the rates of runoff from the major rivers of the world, which are obtained by summing the runoff from all grid boxes in each drainage basin. (For the identification of the drainage basins of the rivers listed in Table 2, see Figure 8.) The percentage change in runoff rate from the control to the global warming experiments is also listed in the table (representing the change in the rate of runoff expected by the year 2050). This table shows that, in high latitudes, runoff from the major rivers such as the Yukon, Mackenzie, and Ob$'$ increases by as much as 20%, whereas runoff from the Yenisey, and Lena increase by 12–13% by the middle of the 21st century.
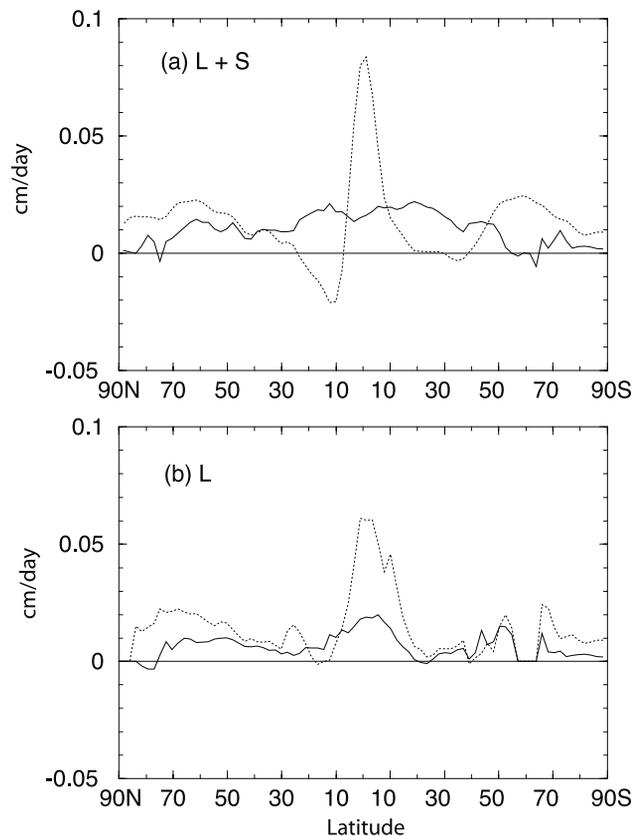
Figure 7. Latitudinal profiles of the simulated zonal mean changes in the annual mean rates of precipitation (dotted line) and evaporation (solid line) from the preindustrial to the middle of the 21st century. Zonal means are taken over an entire latitude circle (a), and over continents only (b). Units are in cm/day.

Table 2. Annual Mean Rates of Simulated Runoff From Major Rivers of the World for the Preindustrial and the Middle (2035–2065 Period) of the 21st Century[a]

	Control	Period	Change, %
High Latitude, 2050 A.D.			
1.Yukon, CA/USA	12.0	14.5	+20.5
2. Mackenzie, CA	9.0	10.8	+20.8
3. Yenisey, Rus.	15.6	17.7	+13.4
4. Lena, Rus.	16.7	18.7	+12.3
5. Ob', Rus.	7.7	9.3	+20.6
Middle Latitude, 2050 A.D.			
6. Rhein	5.2	6.5	+24.5
7. Volga	6.1	7.7	+25.1
8. Danube	7.5	9.1	+20.7
9. Columbia, USA	9.2	11.1	+21.1
10. St. Lawrence, CA	15.2	16.1	+ 6.2
11. Mississippi, USA	11.6	11.7	−
12. Amur, China/Rus.	9.2	9.1	−0.8
13. Yellow, China	16.7	16.8	−
14. Yangtze, China	59.2	61.4	+3.7
15. Zambezi, Zambia	31.1	30.9	−0.7
16. Parana, South America	23.5	29.0	+23.6
Low Latitude, 2050 A.D.			
17. Amazon, S. America	308.	343.	+11.3
18. Orinoco, Col./Venez.	34.3	36.8	+7.5
19. Ganges, Bangl./India	60.7	71.3	+17.5
20. Zaire, Congo	146.	149.	+1.8
21. Nile, Africa	58.3	61.3	−
22. Mekong, Laos/Thai	42.2	39.6	−

[a] In addition, the percentage changes from the preindustrial to the middle of the 21st century are listed. Units are in $10^3 \ m^3 \ s^{-1}$. (For a wide variety of reasons such as the diversion of water for irrigation, the rates of the actual runoff from Yellow, Nile, Mekong, and Mississippi are many times smaller than the simulated rates. For these rivers, percentage changes in runoff are not listed in Table 2.)

[33] In low latitudes, massive runoff from the Amazon, and Ganges increases by 12% and 18%, respectively. The increase in the rate of runoff from the Amazon is attributable mainly to the increase in water vapor content of air accompanying global warning rather than to the intensification of overturning circulation, which hardly changes [*Knutson and Manabe*, 1995]. The large percentage increase in runoff from the Ganges is attributable not only to the increase in absolute humidity of air but also to the increase in the overturning circulation associated with the Indian summer monsoon. In contrast to these rivers, runoff from many other tropical rivers changes by much smaller percentages. For example, runoff from the Zaire and Nile Rivers changes by only a few percent.

[34] In middle latitudes, the rate of runoff from several rivers such as the Volga, Danube, and Rhein Rivers in Europe, the Columbia River in North America and the Parana River in South America increase substantially. However, the rates of runoff from rivers such as the Mississippi, Amur, and Huang He (Yellow) fail to increase substantially (or even decrease slightly).

4. Soil Moisture Change

[35] The geographical distribution of the simulated change in soil moisture, which is expected by the year 2050, is illustrated in Figure 9 for the two 3-month periods of June–July–August, and December–January–February. In middle to high latitudes of the Northern Hemisphere, soil moisture decreases in summer over very extensive regions of both the Eurasian and North American continents with the exception of the extremely arid region, which extends from the Sahara to the Gobi Deserts. The summer reduction of soil moisture is relatively large over the western half of Siberia and northeastern part of North America. On the other hand, soil moisture increases during winter over much of the North American and Eurasian continents.

[36] The physical mechanisms involved in summer dryness in middle to high latitudes of the Northern Hemisphere have been the subject of detailed analysis and extensive discussion in the preceding studies [e.g., *Manabe et al.*, 1981; *Mitchell and Warrilow*, 1987; *Manabe and Wetherald*, 1987; *Wetherald and Manabe*, 1999]. However, the discussion has been focused mainly on summer dryness. Here, we shall briefly discuss the physical mechanisms responsible for not only summer dryness but also winter
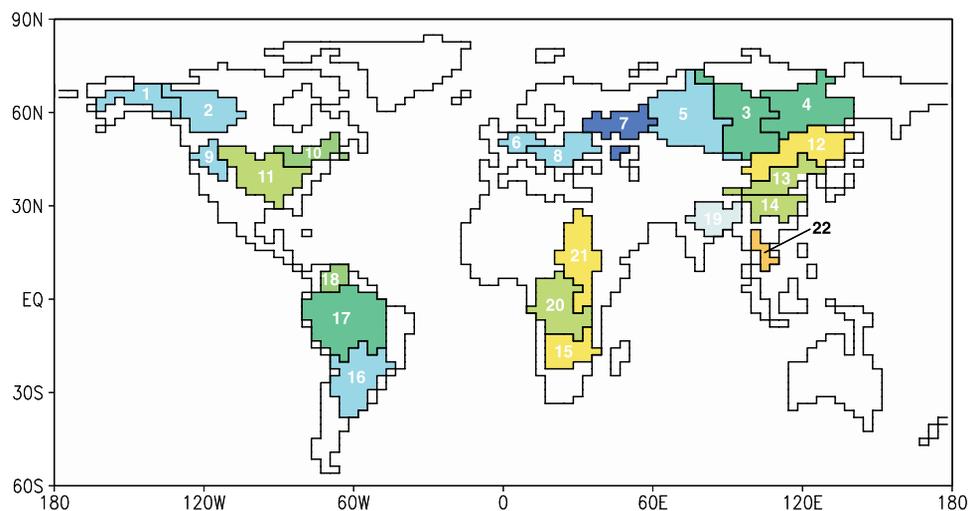
Figure 8. Geographical extents of the major river basins, which are listed in Table 2, are color-coded (personal communication from Christa Dunne). To identify the name of a river, a number is assigned to each basin. It corresponds to the number, which is placed in front of the name of each river listed in Table 2.
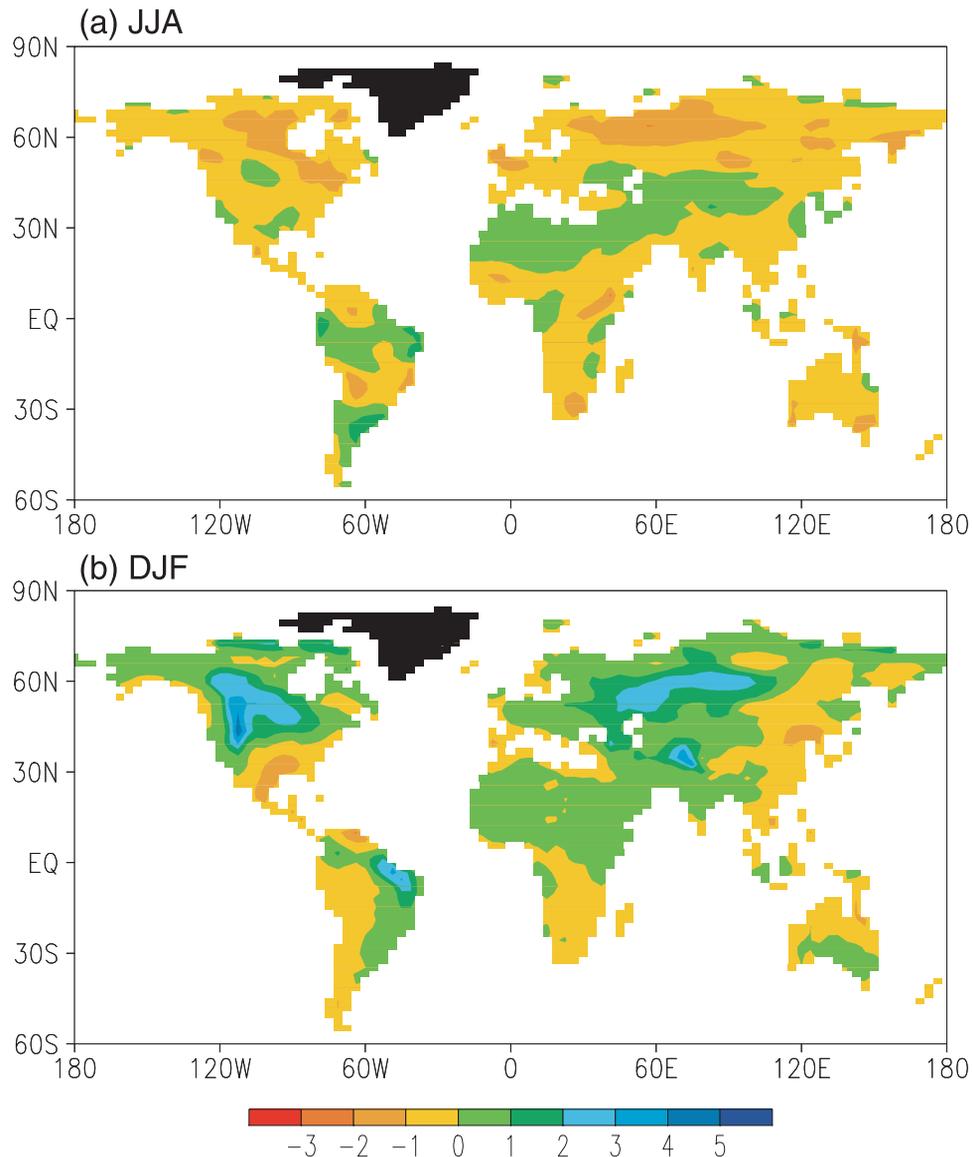
Figure 9. Geographical distributions of the simulated changes in seasonal mean soil moistures (cm) from the preindustrial to the middle of the 21st century. (a) June–July–August (JJA). (b) December–January–February (DJF).

wetness in a coherent manner based upon the analysis in the present as well as the earlier studies mentioned above.

[37] Over oceans, seasonal variation of sea surface temperature (SST) is relatively small. As sea surface temperature increases accompanying global warming, saturation vapor pressure increases at the oceanic surface, thereby enhancing evaporation throughout a year. The increase in oceanic evaporation, in turn, results in the increase in precipitation over continents as water vapor is transported from the ocean to the neighboring continent through the atmospheric circulation.

[38] In sharp contrast to the situation over oceans, surface temperature undergoes a large seasonal variation over continents in middle and high latitudes. The temperature of the continental surface is very low in winter, and high in summer. At low temperatures, saturation vapor pressure hardly increases with increasing temperature due to the nonlinearity of the Clausius-Clapeyron equation. Thus the

heating due to the increase in downward flux of infrared radiation, which results from the increase of greenhouse gases in the atmosphere, contributes mainly to the increase of sensible heat flux rather than that of latent heat of evaporation. This is why the rate of evaporation hardly increases in winter accompanying global warming. On the other hand, precipitation increases over continents due to the increase in the transport of water vapor from the adjacent oceans, where evaporation increases throughout a year. Therefore soil moisture increases in winter as described above.

[39] In summer, when surface temperature and its saturation vapor pressure are high, a major fraction of the heating resulting from the increase in greenhouse gases helps to enhance evaporation. On the other hand, increase in precipitation over the midcontinental regions is not as large as over oceanic regions at a comparable latitude. This is why soil moisture is reduced in summer over very
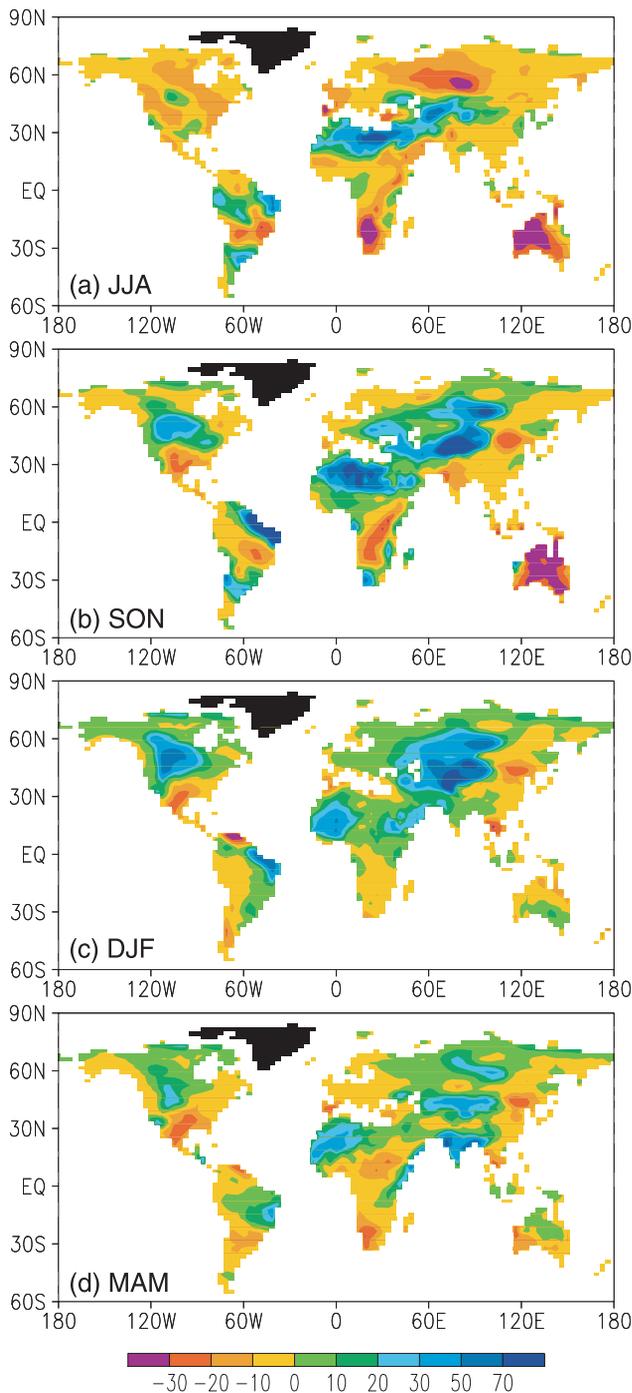
Figure 10. Geographical distributions of simulated, percentage changes in seasonal mean soil moistures from the preindustrial to the middle of the 21st century. (a) June–July–August (JJA). (b) September–October–November (SON). (c) December–January–February (DJF). (d) March–April–May (MAM).

extensive regions in middle to high latitudes of the Northern Hemisphere.

[40] As discussed in our previous studies, there are other important factors that enhance the summer reduction of soil moisture [e.g., *Manabe and Wetherald*, 1987]. In spring, highly reflective snow cover disappears and the soil surface with a relatively low albedo is exposed. Thus the absorption

of solar radiation is enhanced, promoting the evaporation of water from the wet soil surface. As surface temperature increases accompanying global warming, the snowmelt season ends earlier, exposing the soil surface to intense solar radiation. Thus the spring-summer drying of soil moisture begins earlier, thereby enhancing the reduction of soil moisture in summer. In due course, the reduction of soil moisture results in the reduction of evaporation, which reduces the relative humidity in the lower troposphere. The decrease of relative humidity, in turn, reduces rainfall, thereby drying soil further in the late summer.

[41] Over many semi-arid regions in the subtropical and middle latitudes, soil moisture is reduced not only in the June–July–August period, but also in the December–January–February period (Figure 9). To examine this feature of soil moisture change during an entire year, we illustrate in Figure 10 the geographical distributions of the percentage change in soil moisture expected by the middle of the 21st century for four periods of a year, i.e., June–July–August (JJA), September–October–November (SON), December–January–February (DJF), and March–April–May (MAM). It indicates that, accompanying global warming, soil moisture is reduced in many semi-arid regions of the world during much of a year. These regions include the southwestern part of North America, a northeastern province of China in the Northern Hemisphere, and the vicinity of the Kalahari Desert as well as the areas that surround the desert in Australia in the Southern Hemisphere. It is likely that the reduction of soil moisture in these semi-arid regions results in the expansion of many major deserts of the world such as the desert in the southwestern part of North America, the Gobi Desert in Asia, the Kalahari Desert in Africa, and the desert in Australia.

[42] The reduction of soil moisture in these semi-arid regions is also evident in Figure 11a, which illustrates the geographical distribution of the percentage change in annual mean soil moisture. To evaluate the statistical significance of the change in annual mean soil moisture, a "student-t" test is performed. It turns out that most of the annual mean change of soil moisture in the semi-arid regions identified above is statistically significant at the 95% or higher level (Figure 11b). In the following paragraphs, we explore the physical mechanisms responsible for the reduction of soil moisture in these semi-arid regions.

[43] In order to examine how the surface water budget is maintained in a typical semi-arid region, Table 3 is constructed. It tabulates, for both the control and global warming experiments, various components of the surface water budget over an extensive, semi-arid region in the southwestern part of North America. This table shows that, in both the control and global warming experiments, the annual rate of evaporation is equal to the rate of water supply (i.e., precipitation minus runoff), thus maintaining the surface water balance. By the year 2050, the rate of water supply in the semi-arid region decreases from 54.8 cm/yr to 52.0 cm/yr by 5.1%, which is equal to the reduction in evaporation rate.

[44] In a semi-arid region covered by relatively dry air from a nearby desert where air subsides from the upper to lower troposphere, precipitation hardly increases despite the enhanced evaporation from adjacent oceans. On the other hand, the rate of potential evaporation increases due to the
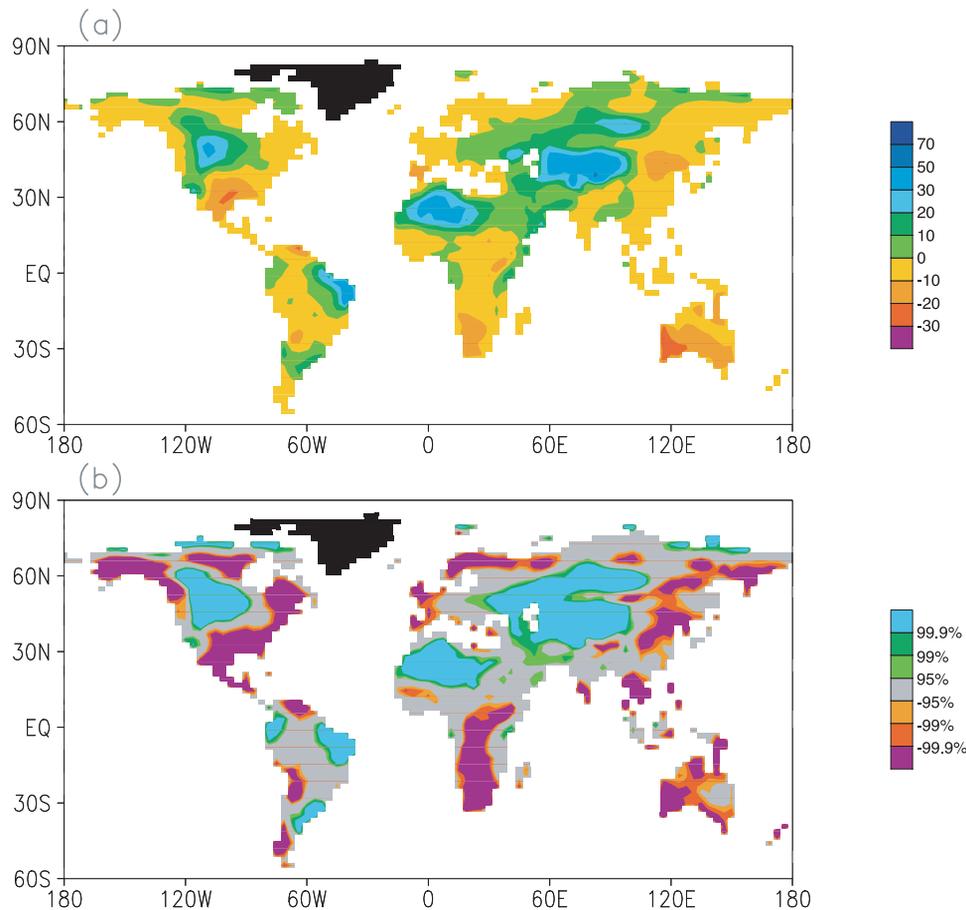
Figure 11. (a) Geographical distributions of simulated, percentage change in annual mean soil moisture from the preindustrial to the middle of the 21st century. (b) Statistical significance of the difference in annual mean soil moisture is color-coded at 95%, 99%, and 99.9% confidence levels.

increase in downward flux of infrared radiation, which occurs in response to the increase of greenhouse gases in the atmosphere. Thus, the balance between evaporation and water supply (i.e., precipitation minus runoff) is maintained at lower level of soil moisture. This is why soil moisture decreases in many semi-arid regions of the world as global warming proceeds.

[45] As soil moisture is reduced, evaporation (from the continental surface) decreases, thereby reducing the relative humidity in the lower troposphere. The reduction of relative humidity, in turn, contributes to the reduction of precipitation, further reducing soil moisture. This is in contrast to the situation over much of the continental regions, where precipitation increases due to the increase of moisture supply from oceanic regions (Figure 12) as discussed earlier.

[46] Figure 10 also indicates that, during JJA and SON, soil moisture is reduced significantly in the savannahs of South America and Africa in the Southern Hemisphere. In the Northern Hemisphere, soil moisture is reduced in Indochina during DJF and MAM, and at the Mediterranean coast of Europe in JJA. In these regions, soil moisture is reduced mainly during the dry season and is hardly reduced during the wet seasons. However, the physical mechanism involved appears to be similar to what is responsible for the reduction of annual mean soil moisture in many semi-arid regions surrounding a desert.

[47] Figure 13 illustrates, for the control experiment and one member of the climate change experiments, a time series of annual mean soil moisture and its 20-year running mean over the semi-arid region in the southwestern part of North America. It shows that, during the latter half of the 20th century, simulated soil moisture in the semi-arid region of North America begins to decrease. Toward the end of the 21st century, the magnitude of the reduction of soil moisture becomes comparable to the standard deviation of its natural variability, which is 0.7 cm, and becomes quite noticeable.

Table 3. Annual Rates of Simulated Precipitation, Runoff, Water Supply (i.e., Precipitation Minus Runoff) and Evaporation, and Soil Moisture Over a Semi-Arid Region in the Southwestern Part of North America for the Preindustrial and the Middle (2035–2065 Period) of the 21st Century[a]

	Control	2050	Change, %
Precipitation	71.1 cm/yr	65.7 cm/yr	−7.5
Runoff	16.3 cm/yr	13.7 cm/yr	−15.8
Water supply	54.8 cm/yr	52.0 cm/yr	−5.1
Evaporation	54.8 cm/yr	52.0 cm/yr	−5.1
Soil moisture	4.40 cm	3.74 cm	−15.0

[a] The region is enclosed by the 20°N and 38°N latitudes, the 88°W and 114°W longitudes, and coastal boundaries. The percentage changes from the preindustrial (the control) to the middle of the 21st century are also listed.
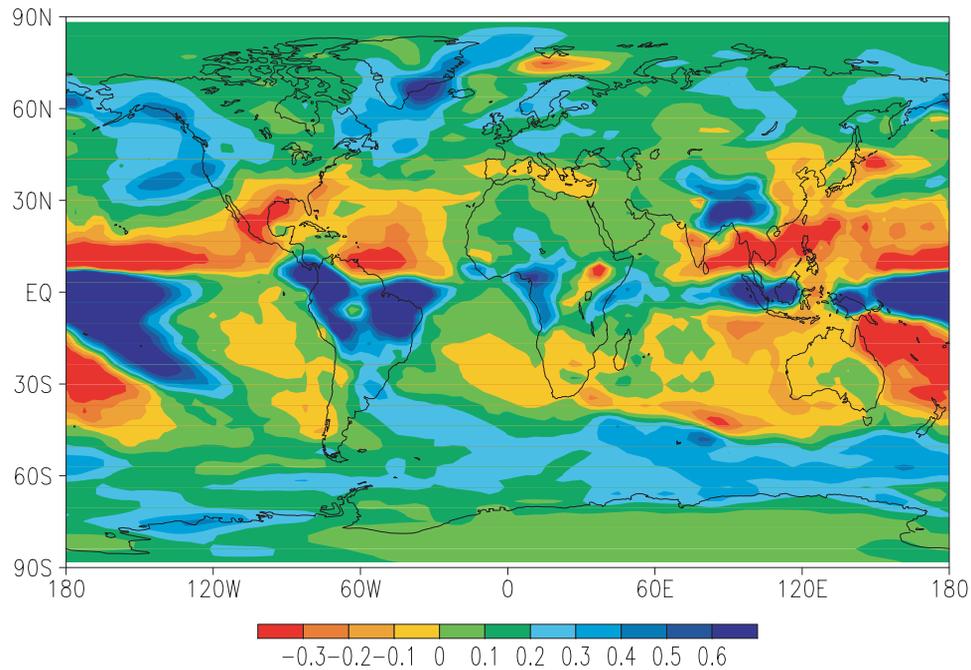
Figure 12. Geographical distribution of the simulated change in annual mean rates of precipitation (cm/day) from the preindustrial to the middle of the 21st century.
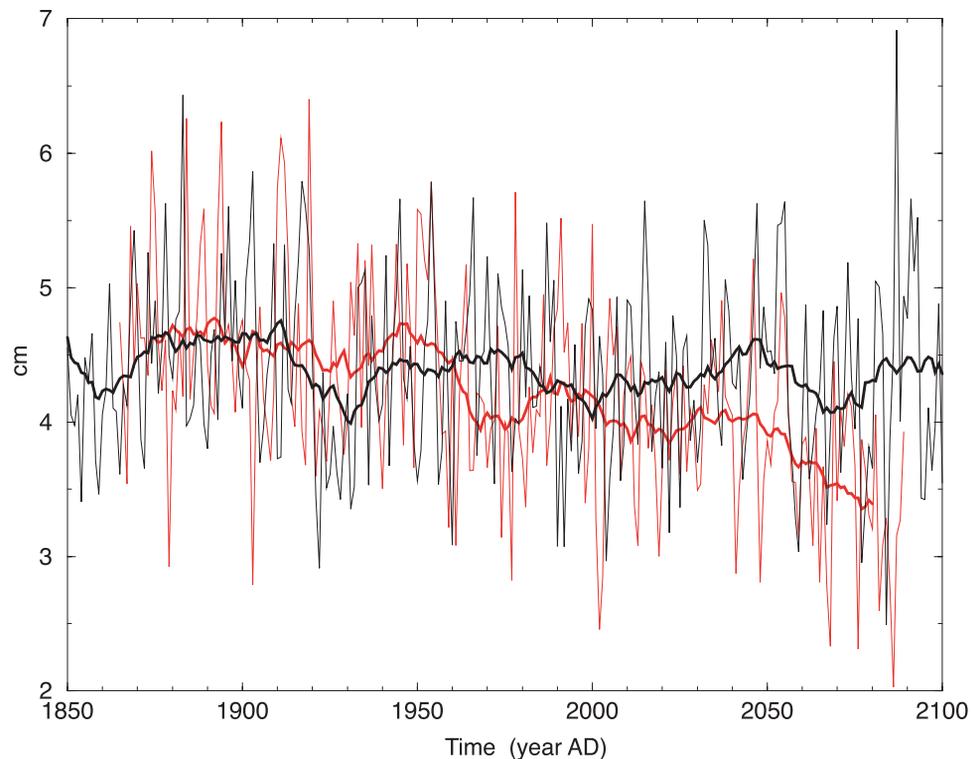
Figure 13. Time series of simulated, annual mean soil moisture (cm) averaged over an extensive semi-arid region in the southwestern part of North America. (The region is enclosed by the 20°N and 38°N latitudes, 88°W and 114°W longitudes, and coastal boundaries.) The thin and thick black solid lines show respectively the time series of annual mean and 20-year running mean soil moisture obtained from the control integration. On the other hand, the thin and thick red lines show respectively the annual mean and 20-year running mean time series of soil moisture obtained from one member of the eight-member ensemble of the climate change experiments.

The major drought with markedly reduced soil moisture occurs more frequently towards the end of 21st century.

[48] In contrast to the situation in many semi-arid regions of the world discussed above, simulated soil moisture increases very slightly during much of a year in the extremely arid region, which extends from the Sahara to Gobi Deserts (see Figures 9 and 10). In this region, soil moisture increases slightly even in summer, when it is reduced over a major fraction of continents in middle to high latitudes.

[49] In this extremely arid region, where soil moisture available for evaporation is practically absent, it is not possible for soil moisture to reduce significantly despite the significant increase in potential evaporation, which results from the increase in downward flux of infrared radiation. On the other hand, precipitation increases very slightly in this region as Figure 12 indicates. Thus, annual mean soil moisture increases very slightly in this region (Figure 10). It is likely, however, that soil moisture quickly evaporates shortly after the end of each rainfall.

[50] The very slight increase in simulated precipitation in this extremely arid region is in contrast to the situation in many semi-arid regions, where precipitation decreases slightly. Since simulated soil moisture is extremely small in this type of region, the changes in evaporation that accompanies the minute change in soil moisture may be too small to reduce the relative humidity of the troposphere enough to reduce precipitation as it did in many semi-arid regions of the world.

5. Summary and Conclusion

[51] A coupled ocean-atmosphere-land surface model with medium computational resolution developed at GFDL produced an improved simulation of the large-scale distributions of precipitation and soil moisture. This encouraged us to use the model for the study of the change in land surface hydrology, which accompanies global warming. The present study describes and discusses the change in land surface hydrology obtained from an eight-member ensemble of the global warming experiments.

[52] The increase in the rate of runoff is particularly large in high northern latitudes, where the runoff from some rivers such as the Mackenzie and Yukon could increase by as much as 20% by the middle of the 21st century. Runoff from many European rivers increases by more than 20%. In some tropical rivers such as the Amazon and Ganges, the rate of runoff also increases substantially. However, the percentage changes in runoff from many tropical rivers and many middle latitude rivers are relatively small.

[53] Over very extensive regions in middle to high latitudes of the Northern Hemisphere, soil moisture decreases in summer, whereas it increases in winter. On the other hand, simulated soil moisture decreases during much of a year in many semi-arid regions of the world, such as the southwestern part of North America, and a northeastern province of China in the Northern Hemisphere. It also decreases in the regions that surround the Kalahari and Australian Deserts in the Southern Hemisphere. The reduction in soil moisture in these semi-arid regions results in the expansion of several major deserts of the world such as the desert in the south-

western part of North America, the Gobi Desert in Asia, the Kalahari Desert in Africa, and the Australian Desert. Soil moisture is also reduced during the dry season in many semi-arid regions of the world. For example, it is reduced in the savannahs of South America and Africa during winter and the early spring in the Southern Hemisphere. In the Northern Hemisphere, it is reduced at the Mediterranean coast of Europe in summer.

[54] In contrast to the semi-arid regions of the world, where soil moisture is reduced during much of a year, soil moisture tends to increase very slightly in the extremely arid region that extends from the Sahara to the Gobi Deserts.

[55] Although there are some significant exceptions (i.e., southern Europe and southeastern United States), the geographical distribution of soil moisture change obtained by *Mitchell and Johns* [1997, Figures 7f and 10f] is broadly consistent with what is obtained in the present study. For example, soil moisture is reduced in summer and increases in winter over extensive regions in middle and high northern latitudes. According to the recent report of the *IPCC* [2001], general drying of the midcontinental areas during summer has also been reproduced using the latest generation of global coupled climate models.

[56] One of the most important factors, which are responsible for the simulated reduction of soil moisture in many semi-arid regions of the world, is the reduction of the annual mean rate of precipitation discussed in the preceding section. Inspecting the map of the multi-model ensemble change of annual mean precipitation recently constructed by IPCC for the scenario IS92a [see *IPCC*, 2001, Figure 9.11c], one notes that, over continents, annual precipitation is reduced over the southwestern part of North America, southern part of Africa, and much of Australia in qualitative agreement with the result from the present study. However, soil moisture does not reduce significantly in the northeastern province of China, differing from the result from the present study.

[57] Our results indicate that the reduction of soil moisture in many semi-arid regions of the world is going to become increasingly noticeable as we go into the latter half of the 21st century. Furthermore, the increase of surface temperature in these regions enhances the evaporation of irrigated water. One of the potential consequences of these changes is the greatly increased demand of water in many semi-arid regions of the world. Unfortunately, river runoff through these semi-arid regions is not projected to increase very much or may even decrease slightly as global warming proceeds. Therefore it is anticipated that, in these semi-arid regions, the shortages of water will be aggravated as we go into the 21st century, posing a very serious challenge for water resource management.

[58] The model used in the present study is simple as compared with many other models, which are currently available. Nevertheless, it simulates approximately the very large-scale features of the geographical distributions of precipitation. The simulated distribution of soil moisture is broadly consistent with the locations of major arid and semi-arid regions of the world. We therefore hope that large-scale distributions of the projected changes in soil moisture and runoff analyzed here are more reliable than what we obtained earlier from the low-resolution version of the model. It is very desirable, however, to confirm the results

obtained in the present study using a model with improved parameterizations of land surface processes.

[59] One should also note that the model used here does not include various biospheric feedbacks, which may be important. For example, the spread of deserts discussed above could lead to changes in the albedo of continental surface. The change in the water balance of soil could also induce a response in plant root systems, leading to changes in effective water-holding capacity of soil [*Milly*, 1997]. Therefore it is very desirable to reevaluate the results obtained here, using a model with biospheric feedback processes.

References

Bryan, K., and L. Lewis, A water-mass model of world ocean, *J. Geophys. Res.*, *84*, 2503–2517, 1979.

Delworth, T. L., R. J. Stouffer, K. W. Dixon, M. J. Spelman, T. R. Knutson, A. J. Broccoli, P. J. Kushner, and R. T. Wetherald, Review of simulations of climate variability and change with the GFDL R30 coupled climate model, *Clim. Dyn.*, *19*, 555–574, 2002.

Gorden, C. T., and W. Stern, A description of the GFDL global spectral model, *Mon. Weather Rev.*, *110*, 625–644, 1982.

Gregory, J. M., and J. F. B. Mitchell, The climate response to CO_2 of Hadley Centre coupled AOGCM with and without flux adjustments, *Geophys. Res. Lett.*, *24*, 1943–1946, 1997.

Haywood, J. M., R. J. Stouffer, R. T. Wetherald, S. Manabe, and V. Ramaswamy, Transient response of a coupled model to estimated change in greenhouse gas and sulfate concentrations, *Geophys. Res. Lett.*, *24*, 1335–1338, 1997.

Intergovernmental Panel on Climate Change (IPCC), The supplementary report to the IPCC Scientific Assessment, in *Climate Change 1992*, edited by J. T. Houghton, B. A. Callander, and S. K. Varney, Cambridge Univ. Press, New York, 1992.

Intergovernmental Panel on Climate Change (IPCC), *IPCC Special Report on Emissions Scenarios*, edited by N. Nakicenovic et al., Cambridge Univ. Press, New York, 2000.

Intergovernmental Panel on Climate Change (IPCC), *Climate Change 2001*: *The Scientific Basis*, edited by J. T. Houghton et al., Cambridge Univ. Press, New York, 2001.

Jones, P. D., and T. M. L. Wigley, Trend '91: A compendium of data on global change, in *Global and Hemispheric Anomalies*, edited by T. A. Boden, R. J. Sepanski, and F. W. Stoss, pp. 512–517, Oak Ridge Natl. Lab., Tenn., 1991.

Knutson, T. R., and S. Manabe, Time-mean response over the tropical Pacific to increased CO_2 in a coupled ocean-atmosphere model, *J. Clim.*, *8*, 2181–2199, 1995.

Knutson, T. R., T. L. Delworth, K. W. Dixon, and R. J. Stouffer, Model Assessment of regional surface temperature trends (1947–1997), *J. Geophys. Res.*, *104*, 30,981–30,996, 1999.

Legates, D. R., and C. J. Willmott, Mean seasonal and spatial variability in gauge-corrected global precipitation, *Int. J. Climatol.*, *10*, 111–127, 1990.

Manabe, S., Climate and ocean circulation, 1, The atmospheric circulation and the hydrology of the earth's surface, *Mon. Weather Rev.*, *97*, 739–774, 1969.

Manabe, S., and R. T. Wetherald, Large-scale change in soil wetness induced by an increase in atmospheric carbon dioxide, *J. Atmos. Sci.*, *44*, 1211–1235, 1987.

Manabe, S., J. Smagorinsky, and R. F. Strickler, Simulated climatology of a general circulation model with a hydrologic cycle, *Mon. Weather Rev.*, *93*, 769–798, 1965.

Manabe, S., R. T. Wetherald, and R. J. Stouffer, Summer dryness due to an increase of atmospheric CO_2 concentration, *Clim. Change*, *3*, 347–386, 1981.

Manabe, S., R. J. Stouffer, M. J. Spelman, and K. Bryan, Transient response of a coupled ocean-atmosphere model to a gradual change of atmospheric CO_2, part I, Annual mean response, *J. Clim.*, *4*, 785–818, 1991.

Manabe, S., M. J. Spelman, and R. J. Stouffer, Transient response of a coupled ocean-atmosphere model to a gradual change of atmospheric CO_2, part II, Seasonal response, *J. Clim.*, *5*, 105–126, 1992.

Marotzke, J., and P. Stone, Atmospheric transport, the thermohaline circulation and flux adjustments in a simple climate model, *J. Phys. Oceanogr.*, *25*, 1350–1364, 1995.

Milly, P. C. D., Potential evaporation and soil moisture in general circulation models, *J. Clim.*, *5*, 209–225, 1992.

Milly, P. C. D., Sensitivity of greenhouse summer dryness to changes in plant rooting characteristics, *Geophys. Res. Lett.*, *24*, 269–271, 1997.

Mitchell, J. F. B., and T. C. Johns, On modification of global warming by sulfate aerosols, *J. Clim.*, *10*, 245–267, 1997.

Mitchell, J. F. B., and D. A. Warrilow, Summer dryness in northern middle latitudes due to increased CO_2, *Nature*, *330*, 238–240, 1987.

Panofsky, H. A., and G. W. Brier, Some applications of statistics in meteorology, Penn. State Univ., State College, Pa., 1968.

Vinnikov, K. Y., A. Robock, R. J. Stouffer, J. E. Walsh, C. L. Parkinson, D. J. Cavalieri, J. F. B. Mitchell, D. Garrett, and V. F. Zakhrov, Global warming and Northern Hemisphere sea ice extent, *Science*, *286*, 1934–1937, 1999.

Wetherald, R. T., and S. Manabe, Detectability of summer dryness caused by greenhouse warming, *Clim. Change*, *43*, 495–511, 1999.

———————————

S. Manabe, Program in Atmospheric and Oceanic Sciences, Princeton University, P. O. Box CN710, Sayre Hall, Forrestal Campus, U.S. Route 1, Princeton, NJ, 08455-0710, USA. (manabe@splash.princeton.edu)

R. W. Wetherald, Geophysical Fluid Dynamics Laboratory, NOAA, Forrestal Campus of Princeton University, Forrestal Road from U.S. Route 1, Princeton, NJ, 08540-9801, USA. (rw@gfdl.noaa.gov)